All-boron analogues of aromatic hydrocarbons: B17− and B18−

Alina P. Sergeeva, Boris B. Averkiev, Hua-Jin Zhai, Alexander I. Boldyrev, and Lai-Sheng Wang

Citation: J. Chem. Phys. **134**, 224304 (2011); doi: 10.1063/1.3599452
View online: http://dx.doi.org/10.1063/1.3599452
View Table of Contents: http://jcp.aip.org/resource/1/JCPSA6/v134/i22
Published by the American Institute of Physics.

All-boron analogues of aromatic hydrocarbons: B_{17}^- and B_{18}^-

Alina P. Sergeeva,[1] Boris B. Averkiev,[1] Hua-Jin Zhai,[2] Alexander I. Boldyrev,[1,a)] and Lai-Sheng Wang[2,b)]
[1]*Department of Chemistry and Biochemistry, Utah State University, 0300 Old Main Hill, Logan, Utah 84322-0300, USA*
[2]*Department of Chemistry, Brown University, Providence, Rhode Island 02912, USA*

(Received 28 February 2011; accepted 20 May 2011; published online 10 June 2011)

We have investigated the structural and electronic properties of the B_{17}^- and B_{18}^- clusters using photoelectron spectroscopy (PES) and *ab initio* calculations. The adiabatic electron detachment energies of B_{17}^- and B_{18}^- are measured to be 4.23 ± 0.02 and 3.53 ± 0.05 eV, respectively. Calculated electron detachment energies are compared with experimental data, confirming the presence of one planar C_{2v} ($^1A_1$) isomer for B_{17}^- and two nearly isoenergetic quasi-planar C_{3v} ($^2A_1$) and C_s ($^2A'$) isomers for B_{18}^-. The stability and planarity/quasi-planarity of B_{17}^- and B_{18}^- are ascribed to σ- and π-aromaticity. Chemical bonding analyses reveal that the nature of π-bonding in B_{17}^- and B_{18}^- is similar to that in the recently elucidated B_{16}^{2-} and B_{19}^- clusters, respectively. The planar B_{17}^- cluster can be considered as an all-boron analogue of naphthalene, whereas the π-bonding in the quasi-planar B_{18}^- is reminiscent of that in coronene. © *2011 American Institute of Physics*. [doi:10.1063/1.3599452]

I. INTRODUCTION

Because of its electron deficiency, boron forms interesting crystal structures dominated by cage-like structural units.[1,2] In recent years, small clusters of boron have received significant attention.[3–47] Earlier computational studies suggested that cage-like boron clusters are not stable,[3–19] rather planar or quasi-planar structures are more favored. Over the past 10 years, we have engaged in an extensive joint photoelectron spectroscopy (PES) and theoretical effort to characterize the structures and bonding of small boron clusters.[20–38] We have shown that small boron cluster anions are indeed planar or quasi-planar. More importantly, we have found that two-dimensional (2D) electron delocalization plays an important role in stabilizing the planar structures and developed the concept of all-boron analogues of aromatic hydrocarbons.[24,25,27,29] It has been shown that the concepts of aromaticity and antiaromaticity can be used to rationalize the chemical bonding, structure, reactivity, and stability of the planar and quasi-planar boron clusters.[20–47] Our initial research has been focused on B_n^- and B_n for $n = 3$–16 and $n = 20$.[21–28] All anions in this size range have been found to be planar or quasi-planar, although the global minimum of neutral B_{20} was found to be a three-dimensional (3D) tubular structure consisting of two B_{10} rings.[28] The transition from 2D to 3D structures was concluded to occur at B_{20} for neutral boron clusters. In a recent study combining density functional theory (DFT) calculations and ion mobility, Oger *et al*. have found that the transition from 2D to 3D structures of boron cluster *cations* occur at B_{16}^+.[39] The size range from B_{17}^- to B_{19}^- has been challenging because of the relative complexity of their PES spectra. In a very recent study,[29] we solved B_{19}^- finally and found that it possesses an unprecedented planar structure with concentric double π-aromaticity, analogous to coronene in its π-bonding pattern.

In the current article, we report an investigation of the structures and chemical bonding of the B_{17}^- and B_{18}^- clusters using PES and *ab initio* calculations. The combined experimental and computational effort shows that a planar C_{2v} ($^1A_1$) global minimum structure is overwhelmingly favored for B_{17}^-, whereas two nearly isoenergetic quasi-planar structures of C_{3v} ($^2A_1$) and C_s ($^2A'$) symmetries are present for B_{18}^-. The two low-lying structures of B_{18}^- are found to be related to the two low-lying structures of B_{19}^-.[29] The corresponding 3D ring-type structures are found to be significantly higher in energy, by 47.5 and 34.0 kcal/mol for B_{17}^- and B_{18}^-, respectively, above the global minimum planar or quasi-planar structures. The stability and planarity/quasi-planarity of B_{17}^- and B_{18}^- are shown again to be due to σ- and π-aromaticity. Chemical bonding analyses revealed that the nature of bonding in B_{17}^- and B_{18}^- is very similar to that in B_{16}^{2-} and B_{19}^-, respectively.[27,29] The B_{17}^- cluster can be viewed as an all-boron analogue of the aromatic naphthalene hydrocarbon molecule as in B_{16}^{2-}, while the π-bonding in the B_{18}^- cluster is reminiscent of that of coronene as in B_{19}^-.

II. EXPERIMENTAL METHOD

The experiment was carried out using a magnetic-bottle PES apparatus equipped with a laser vaporization cluster source, details of which have been described previously.[48] Briefly, the elemental boron anion clusters were produced by laser vaporization of a ^{10}B-enriched (99.75%) disk target in the presence of a pure He carrier gas and analyzed using a time-of-flight mass spectrometer. The B_{17}^- and B_{18}^- clusters of current interest were each mass-selected and decelerated before being photodetached. Two photon energies were used

a)Electronic mail: a.i.boldyrev@usu.edu.
b)Electronic mail: Lai-Sheng_Wang@brown.edu.

in the photodetachment experiment: 266 nm (4.661 eV) and 193 nm (6.424 eV). Photoelectrons were collected at nearly 100% efficiency by the magnetic bottle and analyzed in a 3.5 m long electron flight tube. The PES spectra were calibrated using the known spectra of Rh^- and Au^-, and the energy resolution of the apparatus was $\Delta E_k/E_k \sim 2.5\%$, that is, ~25 meV for 1 eV electrons.

III. THEORETICAL METHODS

We searched for the global minima of B_{17}^- and B_{18}^- using both the Coalescence Kick (CK) method[49–51] and the Basin Hopping (BH) method.[52–55] Both were done initially at the B3LYP level of theory[56–58] using the 3-21G basis set.[59] In the CK method,[49] a random structure is first checked for connectivity: if all atoms in the structure belong to one fragment, then the structure is considered as connected and the normal geometry optimization procedure is applied to it. However, in most cases a randomly generated structure is fragmented, that is, the structure contains several fragments non-bonded with each other including cases with just one atom not being connected. In these cases the coalescence procedure is applied to the fragmented structure — all the fragments are pushed to the center of mass simultaneously. The magnitude of shift should be small enough so that atoms do not approach each other too closely, but large enough so that the procedure converges in a reasonable amount of time. In the current version of the CK program a 0.2 Å shift is used. The obtained structure is checked for connectivity again and the procedure repeats. When two fragments approach each other close enough they "coalesce" to form a new fragment, which will be pushed as a whole in the following steps. Obviously, at some point all fragments are coalesced. This method does not deal with cases when in a randomly generated structure two atoms are too close to each other. To avoid this problem, the initial structures are generated in a very large box with all three linear dimensions being 4* (sum of atomic covalent radii). Hence, usually an initially generated random structure consists of separated atoms as initial fragments. The current version of the program is designed for the global minimum searches of both single molecules of desired composition, and for complexes of molecules like solvated anions (e.g., $SO_4^{2-}.4H_2O$),[60,61] where the initial geometry of each molecular unit is specified in the input file. In the latter case the two molecular units of the complex are considered as connected in a fragment if the distances between two of their atoms are less than the sum of the corresponding van der Waals radii.

BH is an unbiased global minimum search method, in which the potential energy transformation is combined with Monte Carlo sampling.[29,52–55] All low-lying isomers found for B_{17}^- and B_{18}^- by both methods were reoptimized at the B3LYP level using the 6-311+G* basis set,[62–64] with additional single-point calculations at the CCSD(T) level[65–67] using the 6-311+G* basis set and the geometry optimized at the B3LYP/6-311+G* level.

The vertical electron detachment energies (VDEs) were calculated using the restricted outer valence Green's function method [ROVGF/6-311+G(2df)] for B_{17}^- and unrestricted outer valence Green's function method [UOVGF/6-311+G(2df)] (Refs. 68–71) for B_{18}^-, as well as the time-dependent DFT method [TD-B3LYP/6-311+G(2df)] (Refs. 72 and 73) for both anions, all at the optimized B3LYP/6-311+G* geometries. In the latter approach, the first VDE of B_{17}^- was calculated at the B3LYP level as the lowest transition from the singlet state of the anion into the final lowest doublet state of the neutral. Then, the vertical excitation energies of the neutral species (at the TD-B3LYP level) were added to the first VDE to obtain the second and higher VDEs. The first two VDEs of B_{18}^- were calculated at the B3LYP/6-311+G(2df)//B3LYP/6-311+G* level as the lowest transitions from the doublet ground state of the B_{18}^- anion into the final lowest singlet and triplet states of the neutral species at the geometry optimized for the anion. Then the vertical excitation energies calculated at the TD-B3LYP level for the singlet and triplet states of the neutral B_{18} species were added correspondingly to the two lowest VDEs to obtain the higher VDEs of the B_{18}^- anion. Core electrons were frozen in treating the electron correlation at the ROVGF, UOVGF, RCCSD(T), and UCCSD(T) levels of theory.

The B3LYP, RCCSD(T), UCCSD(T), ROVGF, UOVGF, and TD-B3LYP calculations were performed using the GAUSSIAN 03 program.[74] Molecular structure visualization was done using the MOLDEN 3.4 program.[75] Chemical bonding analyses were performed using the Adaptive Natural Density Partitioning (AdNDP) method[76–78] at the B3LYP/3–21G//B3LYP/6-311+G* level. It has been shown previously that the AdNDP results are not sensitive to the level of theory or basis set used.[76,79] Molecular orbital (MO) visualization was performed using MOLEKEL 4.3.[80]

IV. EXPERIMENTAL RESULTS

The photoelectron spectra for B_{17}^- and B_{18}^- are shown in Figs. 1 and 2, respectively, each at 266 and 193 nm. The observed spectral bands are labeled with letters (X, A, B, ...). The vertical lines in Fig. 1(b) for band B represent resolved vibrational structures. The measured adiabatic detachment energies (ADEs) and VDEs are summarized in Tables I and II for the B_{17}^- and B_{18}^- clusters, respectively, where they are compared with theoretical calculations.

A. Photoelectron spectra of B_{17}^-

The 266 nm spectrum of B_{17}^- shows only one broad band (X, Fig. 1(a)), centered at 4.48 eV. This band is likely to contain multiple detachment transitions. Since no vibrational structures are resolved in the threshold region, the ground state ADE is evaluated by drawing a straight line along the leading edge of band X and then adding the instrumental resolution to the intersection with the binding energy axis. Although this is an approximate procedure, we are able to obtain a consistent ADE from the well-defined spectral onsets of band X at different photon energies. The ADE thus evaluated for B_{17}^- is 4.23 ± 0.02 eV.

The 193 nm spectrum (Fig. 1(b)) reveals three additional PES bands at higher binding energies. Band A centered at 4.82 eV partially overlaps with the congested band X.

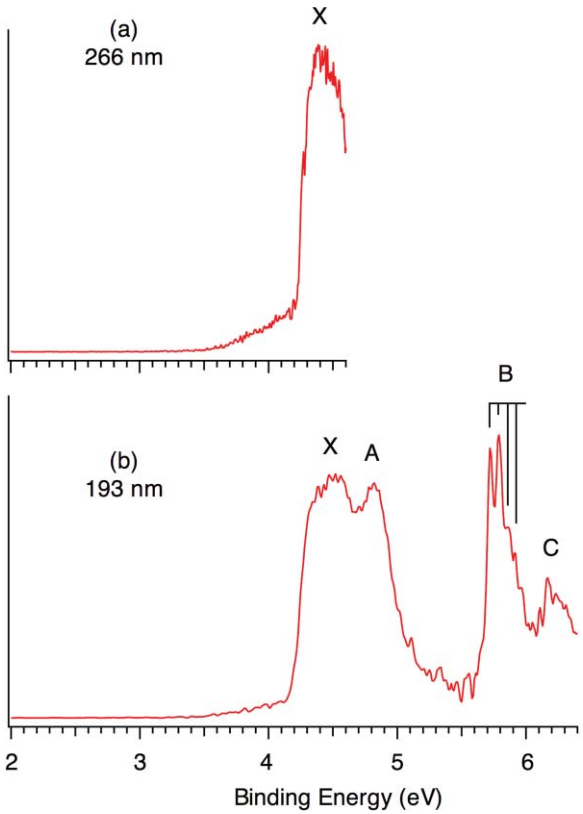

FIG. 1. Photoelectron spectra of B_{17}^- at (a) 266 nm (4.661 eV) and (b) 193 nm (6.424 eV). The vertical bars in (b) represent resolved vibrational structures.

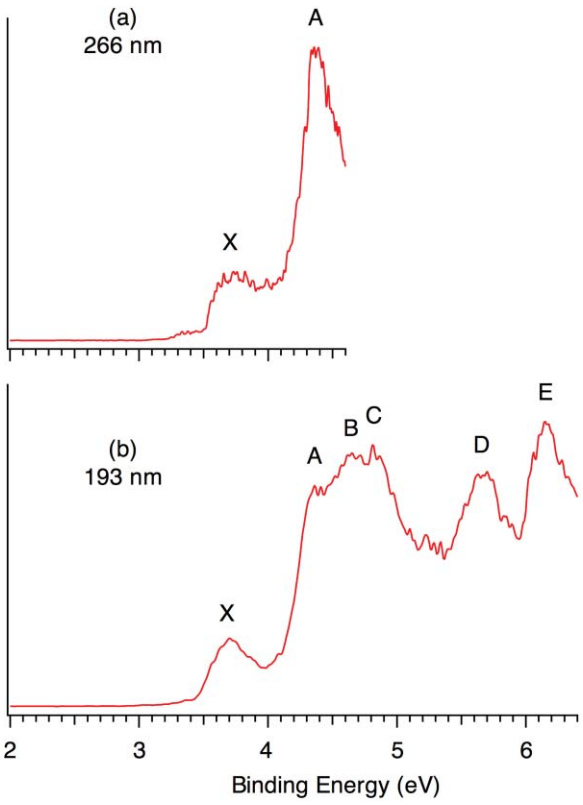

FIG. 2. Photoelectron spectra of B_{18}^- at (a) 266 nm (4.661 eV) and (b) 193 nm (6.424 eV).

Following a large energy gap of 1 eV, band B is vibrationally resolved, whose $0 \leftarrow 0$ and $1 \leftarrow 0$ transitions define the ADE (5.72 eV) and VDE (5.79 eV), respectively, for this excited state transition. The vibrational frequency is measured to be 530 ± 40 cm^{-1}. Band C, centered at 6.22 eV, is relatively weak.

B. Photoelectron spectra of B_{18}^-

The 266 nm spectrum of B_{18}^- (Fig. 2(a)) exhibits two bands: a relatively weak and broad band (X) at a VDE of 3.71 eV and a more intense band (A) at a VDE of 4.38 eV. The ADE for band X is evaluated from its onset to be 3.53 ± 0.05 eV. The width of the X band suggests a large geometry change between the ground state of the B_{18}^- anion and that of the corresponding neutral. Neutral B_{18} has an even number of electrons and the X-A band gap suggests a closed-shell B_{18} neutral cluster with an energy gap of ~0.7 eV between its highest occupied molecular orbital (HOMO) and lowest unoccupied molecular orbital (LUMO). The 193 nm spectrum (Fig. 2(b)) reveals congested electronic transitions between 4 and 5 eV binding energies, where two additional bands B (4.65 eV) and C (4.85 eV) are tentatively identified. Beyond 5 eV, two well-defined bands are observed: D (5.67 eV) and E (6.15 eV). All the PES spectral features of B_{18}^- are fairly broad, suggesting large geometry changes between the anion and the neutral cluster or there may be low-lying isomers contributing to the observed spectra.

V. THEORETICAL RESULTS

A. The global minimum and low-lying structures of B_{17}^-

We searched for the global minimum of B_{17}^- at the B3LYP/3–21G level of theory using the CK and the BH methods. Both programs identified the planar structure I (C_{2v}, $^1A_1$) to be the global minimum of B_{17}^-, as shown in Fig. 3. We then reoptimized the geometry and recalculated the frequencies of the lowest energy isomers at the B3LYP/6-311+G* level. The Cartesian coordinates of the optimized structure of isomer I, as well as its harmonic frequencies and B-B bond lengths, are given in supplementary Tables S1 and S2.[81] The wave function of the global minimum was tested using the stable = opt option as implemented in GAUSSIAN 03 at B3LYP/6-311+G* and found to be stable. Finally, we performed single-point calculations for the two lowest energy isomers, as well as two 3D structures, at the CCSD(T)/6-311+G* level using the optimized B3LYP/6-311+G* geometries. Results of these calculations are given in Fig. 3. The second lowest energy structure, the planar isomer II (C_{2v}, $^1A_1$), was found to be 19.5 kcal/mol above the global minimum (here and elsewhere at the CCSD(T)/6-311+G*//B3LYP/6-311+G* level and with correction for zero-point energy at the B3LYP/6-311+G* level). The two 3D isomers, a tubular structure III (C_s, $^1A'$) and cage-like structure IV (C_{2v}, $^1A_1$), were found to be local minima, but they lie much higher in energy by 47.5 and 69.9 kcal/mol, respectively.

TABLE I. Comparison of the experimental vertical detachment energies (VDEs) with the calculated values of the global minimum structure I (C_{2v}, $^1A_1$) of B_{17}^-. All energies are in eV.

Feature	VDE (expt.)[a]	Final state and electronic configuration	VDE (theo.) TD-B3LYP[b]	OVGF[c]
X[d]	4.48 (5)[e]	$^2B_1$ {…$7b_2^2 2b_1^2 8b_2^2 12a_1^2 9b_2^2 2a_2^2 3b_1^1$}	4.18	4.33 (0.89)
		$^2A_2$ {…$7b_2^2 2b_1^2 8b_2^2 12a_1^2 9b_2^2 2a_2^1 3b_1^2$}	4.28	4.46 (0.89)
		$^2B_2$ {…$7b_2^2 2b_1^2 8b_2^2 12a_1^2 9b_2^1 2a_2^2 3b_1^2$}	4.37	4.41 (0.89)
A	4.82 (3)	$^2A_1$ {…$7b_2^2 2b_1^2 8b_2^2 12a_1^1 9b_2^2 2a_2^2 3b_1^2$}	4.60	4.64 (0.88)
B	5.79 (2)[f]	$^2B_2$ {…$7b_2^2 2b_1^2 8b_2^1 12a_1^2 9b_2^2 2a_2^2 3b_1^2$}	5.70	6.10 (0.88)
C	6.22 (3)	$^2B_1$ {…$7b_2^2 2b_1^1 8b_2^2 12a_1^2 9b_2^2 2a_2^2 3b_1^2$}	6.06	6.05 (0.84)
		$^2B_2$ {…$7b_2^1 2b_1^2 8b_2^2 12a_1^2 9b_2^2 2a_2^2 3b_1^2$}	6.53	6.87 (0.86)

[a]Numbers in parentheses represent the uncertainty in the last digit.
[b]Calculated at the TD-B3LYP/6-311+G(2df)//B3LYP/6-311+G* level.
[c]Calculated at the ROVGF/6-311+G(2df)//B3LYP/6-311+G* level. Values in parentheses represent the pole strength of the OVGF calculation, which characterizes the validity of the one-electron detachment picture.
[d]Adiabatic detachment energy of B_{17}^- is 4.23 ± 0.02 eV.
[e]Estimated from the center of the broad band X, which represents the average of the first three VDEs.
[f]Based on the 1 ← 0 transition. Vibrational frequency: 530 ± 40 cm^{-1}.

B. The global minimum and low-lying structures of B_{18}^-

The search for the global minimum of B_{18}^- using the CK and BH methods at the B3LYP/3–21G level of theory revealed two almost degenerate low-lying isomers, V (C_{3v}, $^2A_1$) and VI (C_s, $^2A'$), as shown in Fig. 4. Geometry reoptimizations and frequency recalculations of the low-lying isomers were performed at the B3LYP/6-311+G* level (see supplementary Tables S3–S6),[81] and single-point calculations were carried out at the CCSD(T)/6-311+G* level of theory using the optimized B3LYP/6-311+G* geometries. At our highest level of theory (CCSD(T)/6-311+G*//B3LYP/6-311+G*), the two isomers V and VI are still close in energy (within 1.6 kcal/mol). The wave functions of the two lowest isomers

TABLE II. Comparison of the experimental VDEs with the calculated values of the global minimum V (C_{3v}, $^2A_1$) and isomer VI (C_s, $^2A'$) of B_{18}^-. All energies are in eV.

Feature	VDE (expt.)[a]	Final state and electronic configuration	VDE (theo.) TD-B3LYP[b]	OVGF[c]
Isomer V (C_{3v}, $^2A_1$)				
X[d]	3.71 (5)	$^1A_1$ {…$7e^4 8e^4 2a_2^2 7a_1^2 9e^4 8a_1^0$}	3.66	3.52 (0.89)
A	4.38 (3)	^3E {…$7e^4 8e^4 2a_2^2 7a_1^2 9e^3 8a_1^1$}	4.15	4.26 (0.89)
		^1E {…$7e^4 8e^4 2a_2^2 7a_1^2 9e^3 8a_1^1$}	4.46	–[e]
B	4.65 (10)	$^3A_1$ {…$7e^4 8e^4 2a_2^2 7a_1^1 9e^4 8a_1^1$}	4.75	4.61 (0.89)
C	4.85 (5)	$^1A_1$ {…$7e^4 8e^4 2a_2^2 7a_1^1 9e^4 8a_1^1$}	4.98	–[e]
D	5.67 (3)	$^3A_2$ {…$7e^4 8e^4 2a_2^1 7a_1^2 9e^4 8a_1^1$}	5.47	5.47 (0.89)
		^3E {…$7e^4 8e^3 2a_2^2 7a_1^2 9e^4 8a_1^1$}	5.44[f]	5.74 (0.86)
		$^1A_2$ {…$7e^4 8e^4 2a_2^1 7a_1^2 9e^4 8a_1^1$}	5.66	–[e]
E	6.15 (3)	^1E {…$7e^4 8e^3 2a_2^2 7a_1^2 9e^4 8a_1^1$}	6.00	–[e]
		^3E {…$7e^3 8e^4 2a_2^2 7a_1^2 9e^4 8a_1^1$}	6.52[f]	6.94 (0.79)
Isomer VI (C_s, $^2A'$)				
A	4.38 (3)	$^1A'$ {$10a''^2 11a''^2 14a'^2 15a'^2 12a''^2 16a'^0$}	4.20	4.41 (0.89)
		$^3A''$ {$10a''^2 11a''^2 14a'^2 15a'^2 12a''^1 16a'^1$}	4.24	4.42 (0.89)
		$^3A'$ {$10a''^2 11a''^2 14a'^2 15a'^1 12a''^2 16a'^1$}	4.29	4.40 (0.89)
B	4.65 (10)	$^1A''$ {$10a''^2 11a''^2 14a'^2 15a'^2 12a''^1 16a'^1$}	4.50	–[e]
		$^3A'$ {$10a''^2 11a''^2 14a'^1 15a'^2 12a''^2 16a'^1$}	4.50	4.41 (0.89)
		$^1A'$ {$10a''^2 11a''^2 14a'^2 15a'^1 12a''^2 16a'^1$}	4.56	–[e]
		$^3A''$ {$10a''^2 11a''^1 14a'^2 15a'^2 12a''^2 16a'^1$}	4.60	4.66 (0.89)
C	4.85 (5)	$^1A'$ {$10a''^2 11a''^2 14a'^1 15a'^2 12a''^2 16a'^1$}	4.82	–[e]
		$^1A''$ {$10a''^2 11a''^1 14a'^2 15a'^2 12a''^2 16a'^1$}	4.85	–[e]
E	6.15 (3)	$^3A''$ {$10a''^1 11a''^2 14a'^2 15a'^2 12a''^2 16a'^1$}	6.03	6.32 (0.85)

[a]Numbers in parentheses represent the uncertainty in the last digits.
[b]Calculated at the TD-B3LYP/6-311+G(2df)//B3LYP/6-311+G* level.
[c]Calculated at the UOVGF/6-311+G(2df)//B3LYP/6-311+G* level. Values in parentheses represent the pole strength, which characterizes the validity of the one-electron detachment picture.
[d]Adiabatic detachment energy of B_{18}^- is 3.53 ± 0.05 eV.
[e]These values cannot be calculated at this level of theory.
[f]Multiconfigurational value.

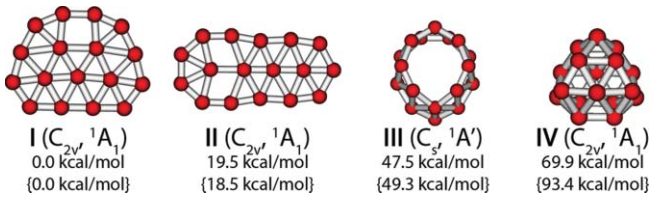

FIG. 3. The planar global minimum of the B_{17}^- cluster (isomer I) and its representative higher energy isomers, which have planar (isomer II), tubular (isomer III), and cage-like (isomer IV) geometries. Geometry optimization was performed at the B3LYP/6-311+G* level of theory. Relative energies are given at the CCSD(T)/6-311+G*//B3LYP/6-311+G* level and B3LYP/6-311+G* level (in curly brackets), both corrected for zero-point vibrational energies calculated at the B3LYP/6-311+G* level. It should be noted that the solid rods do not necessarily represent a single B-B bond between boron atoms. The relatively short B-B distances (<2.0 Å) were connected to help with the visualization of the cluster structures.

V and VI were found to be stable at B3LYP/6-311+G* using the stable = opt option as implemented in GAUSSIAN 03. Alternative isomers VII–X were found to be appreciably higher in energy (by 8.5–34.0 kcal/mol).

The lowest energy structure of B_{18}^- is quasi-planar with a C_{3v} symmetry. The central B_3 unit is slightly out of plane (located ~0.5 Å above the plane of the molecule), reminiscent of the bowl structure of B_{12},[25] which also has C_{3v} symmetry featuring a B_9 ring and an out-of-plane central B_3 unit. Isomer VI is only 1.6 kcal/mol higher in energy and also possesses a quasi-planar structure. It has a nice bowl shape, consisting of a B_{12} outer ring, a slightly out-of-plane B_5 inner ring capped by a central apex atom.

VI. COMPARISON BETWEEN THE EXPERIMENTAL PHOTOELECTRON SPECTRA AND CALCULATED ELECTRON DETACHMENT ENERGIES

A. B_{17}^-

According to the computed energies (Fig. 3), isomer I (C_{2v}, $^1A_1$) of B_{17}^- is overwhelmingly favored and should be the only one considered for comparison with the experimental data. The calculated VDEs for isomer I at the TD-B3LYP/6-311+G(2df) and ROVGF/6-311+G(2df) levels of theory are compared with the experimental VDEs in Table I. The pole strengths are also given in the parentheses for the calculated VDEs at the OVGF level, providing indications for the validity of the single-particle description of the photodetachment processes. A pole strength exceeding 0.87 suggests the greatest validity for the one-electron detachment picture. Since the anion is a closed-shell system, electron detachment from each valence MO will generate a single final doublet electronic state within the one-electron picture. The calculated VDEs for the first three transitions into the $^2B_1$, $^2A_2$, and $^2B_2$ final states are very close to each other, averaging at 4.28 and 4.40 eV at the B3LYP and OVGF levels, respectively. These calculated spectral patterns are in excellent agreement with the experimental spectra. The three transitions overlap with each other, resulting in the broad feature X centered at 4.48 eV (Table I and Fig. 1). It should be noted that there are very subtle and minor changes in geometry upon ejection of an electron from the C_{2v} structure of the B_{17}^- anion to the lowest doublet state of the corresponding neutral species (see pages 9 and 10 in the supplementary material for the supporting data).[81]

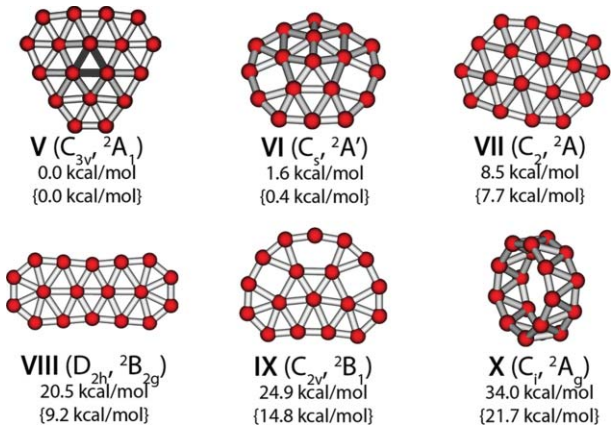

FIG. 4. The global minimum and representative higher energy isomers for the B_{18}^- cluster. Geometry optimization was performed at the B3LYP/6-311+G* level of theory. Relative energies are given at the CCSD(T)/6-311+G*//B3LYP/6-311+G* level and B3LYP/6-311+G* level (in curly brackets), both corrected for zero-point vibrational energies calculated at the B3LYP/6-311+G* level.

The fourth transition into the $^2A_1$ final state (VDE at TD-B3LYP: 4.60 eV; VDE at OVGF: 4.64 eV with the pole strength of 0.88) is assigned to feature A (4.82 eV), whereas the fifth transition into the final $^2B_2$ state (VDE at TD-B3LYP: 5.70 eV; VDE at OVGF: 6.10 eV with the pole strength of 0.88) is responsible for the vibrationally resolved band B with a measured VDE of 5.79 eV. The large energy gap between features A and B is nicely reproduced in the theoretical calculations. There is a totally symmetric normal mode of the B_{17}^- anion, which could be correlated with the measured vibrational frequency of 530 ± 40 cm^{-1} for the neutral species in the B band corresponding to the final $^2B_2$ state: $\omega_{12}(a_1)$ = 532 cm^{-1} (for the full list of the calculated harmonic frequencies see supplementary Table S2).[81] This mode was found to have about the same frequency in the lowest $^2B_1$ state of the neutral B_{17} cluster: 531 cm^{-1}. We could not optimize the neutral B_{17} cluster in the second excited spectroscopic state of $^2B_2$ symmetry, but we think that the $\omega_{12}(a_1)$ vibrational mode will be approximately the same in this state. The calculated $\omega_{12}(a_1)$ frequency corresponds to a totally symmetric "breathing" normal mode. Finally, the sixth transition into the $^2B_1$ final state (VDE at TD-B3LYP: 6.06 eV; VDE at OVGF: 6.05 eV with the pole strength of 0.84) is responsible for the experimental feature C at 6.22 eV. The next detachment channel occurs at 6.53 eV according to TD-B3LYP and 6.87 eV according to OVGF calculations (with the pole strength of 0.86), which is beyond the 193 nm photon energy. The overall calculated spectral patterns at both TD-B3LYP and OVGF are in qualitative agreement with the experimental PES spectra, lending considerable credence to the global minimum of B_{17}^- identified from the theoretical calculations.

B. B_{18}^-

The global minimum searches for B_{18}^- revealed two nearly degenerate isomers, V (C_{3v}, $^2A_1$) and VI (C_s, $^2A'$) (Fig. 4). Within the accuracy of the theory, it is difficult to decide which one is the true global minimum. Thus, both

isomers might be present in our cluster beam and contribute to the experimental PES spectra shown in Fig. 2. As will be seen below, we have strong evidence that, in addition to isomer V, isomer VI was also present experimentally. The calculated VDEs for isomers V and VI at the TD-B3LYP/6-311+G(2df) and ROVGF/6-311+G(2df) levels of theory are compared with the experimental data in Table II.

1. Isomer V

The first detachment channel from isomer V is from the singly occupied $8a_1$ orbital into the closed shell singlet $^1A_1$ final state of neutral B_{18}. The calculated VDE for this channel is 3.66 eV at TD-B3LYP and 3.52 eV at OVGF (with the pole strength of 0.89); both are in reasonable agreement with the first observed PES band (VDE = 3.71 eV) (Table II). The relatively low intensity of the experimental feature X (Fig. 2) is consistent with the transition into the final singlet state. The second calculated VDE of isomer V (VDE at TD-B3LYP: 4.15 eV; VDE at OVGF: 4.26 eV with the pole strength of 0.89) corresponds to a final triplet state (^3E) with electron detachment from the 9e orbital (HOMO–1) (Table II), which is in good agreement with the experimental VDE of band A of 4.38 eV. The relatively high intensity of feature A is also consistent with the electron detachment from the doubly degenerate HOMO–1 into a final triplet state. The X-A bands define a HOMO-LUMO gap of ~0.7 eV for neutral B_{18}, which is qualitatively borne out from the calculated VDEs. Using OVGF, we cannot calculate the VDEs for the singlet excited states, which are expected to yield detachment features with weaker intensities, as shown by the first detachment channel. Thus, in the following discussion we will focus mainly on transitions to the final triplet states, which should dominate the PES spectra. The broad spectral width and congested nature of all the observed features beyond 4 eV is partly due to the fact that both triplet and singlet final states can be produced from detachment from fully occupied orbitals of B_{18}^- (all orbitals below the singly occupied HOMO).

The next transition into a final triplet state ($^3A_1$) comes from detachment from the $7a_1$ orbital (HOMO–2) with a calculated VDE of 4.75 at TD-B3LYP and 4.61 eV at OVGF with the pole strength of 0.89, in good agreement with the observed VDE for band B (4.65 eV) (Table II). The corresponding singlet final state yields a calculated VDE of 4.98 eV at TD-B3LYP, which should contribute to band C. The next two detachment channels come from the $2a_2$ and 8e orbitals, giving VDEs very close to each other (5.47 and 5.44 eV at TD-B3LYP; 5.47 and 5.74 eV at OVGF), in good agreement with band D with a measured VDE of 5.67 eV. The singlet final state from the 8e orbital yields a VDE of 6.00 eV at TD-B3LYP, which should contribute to band E at 6.15 eV. The detachment channel from the 7e orbital to the ^3E final state yields a VDE of 6.52 eV at TD-B3LYP and 6.94 eV at OVGF (with the low pole strength value of 0.79), which is beyond our photon energy at 193 nm.

2. Isomer VI

The calculated VDE values of isomer VI are significantly higher (Table II) and they would be all overlapped with the features from isomer V if isomer VI were present experimentally. The VDEs for the first three detachment channels for isomer VI are very close in energy and would contribute to band A. The next four detachment channels yield VDEs very close to each other and they would all contribute to band B. The most convincing evidence that isomer VI was present in the PES experiment comes from bands C and E. Both of these bands correspond to singlet detachment channels from isomer V. However, their relatively high intensities suggest that they have contributions from isomer VI. The eighth and ninth detachment channels from isomer VI give VDEs of 4.82 and 4.85 eV at TD-B3LYP, in good agreement with that of band C. The last calculated detachment channel from isomer VI is from the 10a" orbital, with a calculated VDE of 6.03 eV at TD-B3LYP and 6.32 eV at OVGF, in excellent agreement with band E. All the VDEs calculated for Isomer VI at the OVGF level exhibit pole strengths of 0.85 and higher.

In summary, the broad and complicated PES spectral features of B_{18}^- are consistent with the presence of two isomers. Overall, the calculated spectral patterns of isomers V and VI together are in very good agreement with the observed PES spectra, providing credence to the theoretical calculations that these two isomers are close in energy. The quasi-planarity of isomers V and VI suggests that these structures are likely to be fairly floppy, which is consistent with the broad PES features observed for B_{18}^-. It is noted that isomer VI possesses a very small or no HOMO-LUMO gap. Hence, a closed-shell B_{18}^{2-} for isomer VI is expected to be a stable species, which may be produced in the form of LiB_{18}^- [$Li^+(B_{18}^{2-})$], as observed previously for smaller boron clusters.[30,31]

VII. STRUCTURES AND CHEMICAL BONDING

A. B_{17}^-: An all-boron naphthalene

1. Structural stability of the planar B_{17}^-

The good agreement between the calculated VDEs and the PES data and the relatively clean PES spectra (Fig. 1) confirm convincingly about the C_{2v} planar structure I as the global minimum of B_{17}^- (Fig. 3). This structure is very different from the global minimum of the B_{17}^+ cation,[39] which was identified to be a tubular structure similar to isomer III or to the global minimum of neutral B_{20}.[28] As shown in Fig. 3, the tubular structure in the anion is 47.5 kcal/mol higher in energy than the global minimum C_{2v} planar structure. In fact, the planar C_{2v} global minimum structure of B_{17}^- is so overwhelmingly favored that even the closest low-lying isomer is still 19.5 kcal/mol higher. It is surprising that the relative energies of the planar structure I and tubular structure III are so different in the two charge states.

2. An all-boron naphthalene

To understand the stability of the planar B_{17}^- cluster, we performed chemical bonding analyses based on the canonical molecular orbitals (CMOs) and the AdNDP method.[76] We found that B_{17}^- possesses five fully occupied π-orbitals with 10 π-electrons. In fact, the π-orbitals of B_{17}^- are very sim-

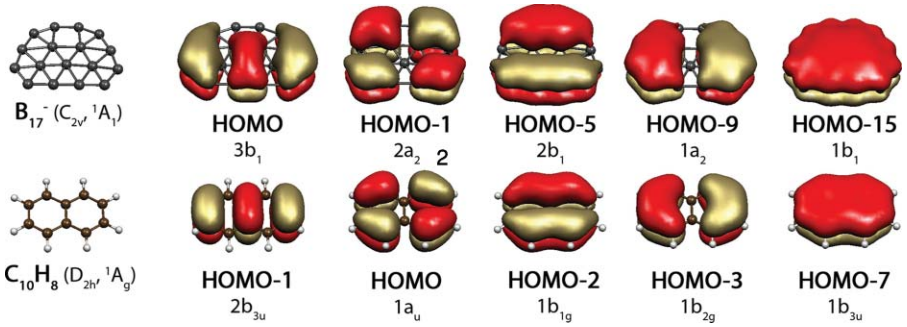

FIG. 5. Comparison of the π-bonding patterns of B_{17}^- (C_{2v}, $^1A_1$) and $C_{10}H_8$ (D_{2h}, ^1A_g).

ilar to those of the aromatic naphthalene molecule ($C_{10}H_8$), as shown in Fig. 5. Thus, B_{17}^- is a $\pi-$aromatic system and should be considered as a new member of the growing family of hydrocarbon analogues of boron clusters.[24,25,27,29] Naphthalene is a prototypical aromatic molecule with its 10 π-electrons satisfying the $(4n + 2)$ Hückel rule for π-aromaticity ($n = 2$). The remarkable similarity between the π-systems of naphthalene and B_{17}^- suggests that the B_{17}^- cluster can be viewed as an "all-boron naphthalene" like B_{16}^{2-}, which also has a set of five π-orbitals nearly identical to that of naphthalene.[27]

However, it is more difficult to discuss the σ-bonding in such a large system as B_{17}^- using the CMOs. It has been shown that the σ-density can be successfully analyzed using the AdNDP method for B_{16}^{2-} and B_{19}^-.[27,29] The 52 valence electrons (including the 10 π-electrons) in B_{17}^- comprise 26 valence CMOs, which are transformed into 26 localized/delocalized chemical bonds using the AdNDP analysis (Fig. 6). The occupation numbers (ONs) indicate the number of electrons per bond, and the ONs of all the recovered bonding elements in B_{17}^- are close to the ideal limit of 2.0 |e|. The localized bonding in B_{17}^- as revealed by AdNDP is represented by 12 two-center two-electron (2c-2e) peripheral B-B σ-bonds. The rest of the electron density is delocalized. There are 9 delocalized σ-bonds: five being delocalized over three atoms and four over four centers. If one

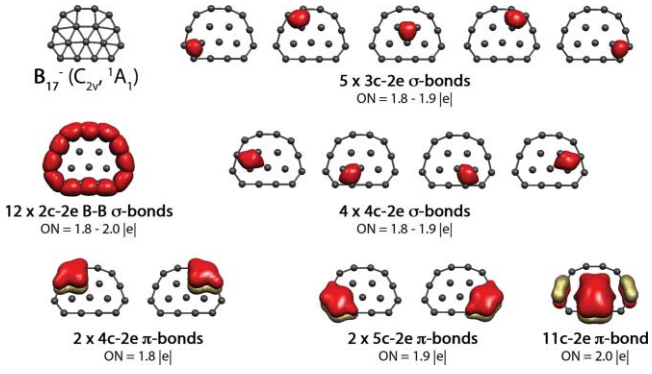

FIG. 6. Results of the Adaptive Natural Density Partitioning analyses on the chemical bonding in the global minimum structure I (C_{2v}, $^1A_1$) of B_{17}^-. Each bond revealed through the analysis is localized/delocalized on n centers and it is composed of either 2 electrons (nc-2e bond; doubly occupied bond) or one electron (nc-1e; singly occupied bond). The ON stands for occupation number, which is equal to 2 electrons (2.0 |el) in ideal cases of doubly occupied bonds and 1 electron (1.0 |el) in case of a singly occupied bond.

applies the $(4n + 2)$ rule to this σ-bonding pattern, the B_{17}^- cluster can be considered as σ-aromatic ($4n + 2 = 18$; $n = 4$).

The prototypical B-B σ-bond is 1.629 Å at the B3LYP/6-311++G** level of theory.[82] The calculated B-B distances in B_{17}^- are within the range of a single bond for the peripheral B-B bonds (see supplementary Table S2).[81] All the interior B-B distances are larger. These results support our chemical bonding picture: the peripheral boron atoms form single 2c-2e bonds, whereas the boron atoms inside the peripheral ring are held by delocalized bonds only.

The AdNDP method also recovered five delocalized π-bonds: two 4c-2e π-bonds, two 5c-2e π-bonds, and one 11c-2e π-bond. These π-bonds are very similar to those revealed in naphthalene through the AdNDP analysis,[77] further confirming that the B_{17}^- cluster is an all-boron analogue of $C_{10}H_8$ and showing the consistency between the CMO and AdNDP bonding analyses. Therefore, the stability of the perfectly planar C_{2v} ($^1A_1$) global minimum of B_{17}^- can be attributed to its double σ- and π-aromaticity.

B. B_{18}^-: An all-boron analogue of coronene

1. Structural similarity between B_{18}^- and B_{19}^-

We have both experimental and theoretical evidence that B_{18}^- possesses two close isomers (isomers V and VI) competing for the global minimum. Both isomers are quasi-planar (Fig. 4) and are related to the two low-lying structures of B_{19}^-. We have reported recently that B_{19}^- possesses two close-lying isomers.[29] The global minimum of B_{19}^- is a concentric doubly π aromatic planar cluster (C_{2v} symmetry) consisting of a 13-atom outer ring, a 5-atom inner pentagonal ring, plus a central B atom. Molecular dynamics simulations have shown that the inner pentagonal ring and the outer ring can almost freely rotate against each other, forming a molecular "Wankel motor."[83] Isomer VI of B_{18}^- is very similar to the global minimum of B_{19}^-, consisting of a 12-atom outer ring, a 5-atom pentagonal ring, plus a central B atom. It can be viewed as removing a B atom from the 13-atom outer ring of the global minimum of B_{19}^-. However, the 12-atom ring in B_{18}^- is apparently too small to fit the inner six B atoms, "squeezing" the pentagonal ring and the central B atom slightly out of plane. Thus, the quasi-planarity in isomer VI of B_{18}^- can be viewed as a "mechanical" effect, which has also been observed in smaller boron clusters, such as B_7^- and

B_{12}^-.[25,26] Recently, we have shown that substitution of one B atom by an Al atom from the outer ring in B_7^- and B_{12}^- is sufficient to induce planarity by slightly expanding the outer ring due to the larger size of Al.[84] In the case of B_{18}^-, we can see that insertion of one more B atom in its outer ring creates enough room to fit the central six B atom in a perfect planar structure.[29]

The B_{19}^- cluster also possesses a low-lying planar isomer (again of C_{2v} symmetry), which is only 3.7 kcal/mol higher in energy than the concentric planar global minimum at the CCSD(T) level of theory.[29] This isomer of B_{19}^- has a triangular shape consisting of a 13 peripheral B atoms and a nearly perfect B_6 triangle in the center. Isomer V of B_{18}^- can be viewed as removing a peripheral B atom from this low-lying isomer of B_{19}^-. The reduced outer ring then "squeezes" the central B_3 triangle out of plane in isomer V of B_{18}^-, very similar to the "mechanically" induced nonplanarity in isomer VI. It is interesting that isomer V of B_{18}^- has C_{3v} symmetry and all remaining 15 B atoms are almost in the same plane. Clearly, the insertion of one more B atom into the periphery of isomer V of B_{18}^- leads to the perfect planar low-lying isomer of B_{19}^-.

We also note that the two low-lying structures of B_{18}^- are quite different from the global minimum of the B_{18}^+ cation, for which the double ring tubular structure was found to be the global minimum.[39] The tubular isomer for B_{18}^- is 34 kcal/mol higher in energy than the global minimum isomer V (Fig. 4).

2. An all-boron analogue of coronene

To understand the bonding in the two low-lying isomers of B_{18}^-, we carried out both CMO and AdNDP analyses. In the strict sense the notation of irreducible representations (such as σ-, π-, δ-, ϕ-, etc.) can be applied to CMOs of linear molecules only. Nevertheless, this notation is widely used in chemistry to explain chemical bonding in molecules of nonlinear point groups, mainly in planar or quasi-planar molecules. For molecules composed of main group elements such as the planar boron clusters, there are two types of CMOs: σ and π, where σ-CMOs do not have a nodal plane and π-CMOs have one nodal plane coinciding with the plane of the molecule. In cases of nonplanar molecules, significant mixing of σ- and π-electron density occurs. In the case of quasi-planar molecules, in which the out-of-plane distortion is small, it is still possible to attribute CMOs to either σ- or π-symmetry. Both isomers V and VI of B_{18}^- can be considered to be quasi-planar because their out-of-plane distortions are small.

Isomer V has the following electronic configuration: $1a_1^2 1e^4 2a_1^2 2e^4 1a_2^2 3e^4 3a_1^2 4e^4 4a_1^2\ 5e^4 5a_1^2 6a_1^2 6e^4 7e^4 8e^4 2a_2^2 7a_1^2 9e^4 8a_1^1$. In order to identify more clearly the CMOs with π-symmetry for the quasi-planar B_{18}^- cluster, we also computed the CMOs for the D_{3h} B_{18}^- by flattening the cluster artificially. The π-type CMOs for both the quasi-planar and the planar B_{18}^- are compared in Fig. 7(a). Six π-CMOs are found for isomer V: two pairs of doubly degenerate orbitals of e symmetry (HOMO–1 and HOMO–1′; HOMO–6 and HOMO–6′) and two orbitals of a_2 symmetry (HOMO–3 and HOMO–14). The electronic configuration of the low-lying isomer VI of B_{18}^- is: $1a'^2 2a'^2 1a''^2 3a'^2 2a''^2 4a'^2 5a'^2 3a''^2 6a'^2 4a''^2 5a''^2 7a'^2 8a'^2 6a''^2\ 9a'^2 10a'^2 7a''^2 11a'^2 8a''^2 12a'^2 9a''^2\ 13a'^2 10a''^2 11a''^2 14a'^2 15a'^2\ 12a''^2 16a'^1$. Its six π-CMOs, HOMO (16a′), HOMO–1 (12a″), HOMO–3 (14a′), HOMO–7 (9a″), HOMO–8 (12a′), and HOMO–15 (8a′), are displayed in Fig. 7(b) and correlated with those of the flattened structure (C_{2v}, $^2B_1$). As shown in Fig. 7, the CMOs of isomers V and VI of B_{18}^- are not significantly different from those of the flattened structures due to the very small out-of-plane distortions.

The π-CMOs for both isomers are very similar to each other and they are both similar to those of the concentric B_{19}^- cluster.[29] The π-CMOs can be categorized into two classes, one delocalized on the central six B atoms, and five π CMOs describing bonding between the central B atoms with the periphery. Thus, both isomers possess two concentric π-systems, similar to B_{19}^-, and can be viewed as all-boron analogues of coronene.[29] However, there is one significant difference between the π-CMOs of isomers V and VI. In isomer VI, the HOMO is a π-CMO, which is half occupied. Thus, strictly speaking, only the closed-shell doubly charged B_{18}^{2-} cluster is doubly aromatic for isomer VI. This is likely the reason why isomer VI has a high first VDE and very small HOMO-LUMO gap and why it is slightly less stable than isomer V, which possesses a set of fully occupied π-CMOs. As mentioned above, we expect the doubly charged isomer VI to be highly stable and it may be observed as LiB_{18}^-, similar to LiB_6^- and LiB_8^-.[30,31]

We present the AdNDP analysis for the lowest energy C_{3v} isomer V of B_{18}^- only, since the π-bonding patterns of isomers V and VI are quite similar (Fig. 7). The current version of our AdNDP program can only deal with closed-shell systems. Therefore, in order to assess chemical bonding in the open-shell B_{18}^- anion cluster, we performed AdNDP analyses of the closed-shell B_{18}^{2-} dianion and neutral B_{18} at the geometry of isomer V of B_{18}^-. As in all other pure boron clusters previously studied by AdNDP, only the peripheral boron atoms in B_{18}^- are involved in classical localized 2c-2e B-B σ-bonding (Fig. 8), as also shown in Fig. 6 for B_{17}^-. The extra electron in isomer V of B_{18}^- is clearly delocalized over the central B_3 triangle and the ON of this bond is 1.0 |e|. There is also a delocalized π-bond over the central B_6 triangle. The remaining nine delocalized σ-bonds are all 3c-2e bonds as well, being responsible for the bonding between the inner six B atoms and the 12-atom outer ring. This set of nine 3c-2e σ-bonds satisfies the $(4n + 2)$ Hückel rule, rendering the system σ-aromatic ($n = 4$). The 10 π-electrons occupying the set of five π-bonds (three 5c-2e and two 18c-2e) satisfy the $(4n + 2)$ rule for π-aromaticity ($n = 2$). This set of π-bonds is primarily responsible for the π-bonding between the inner six B atoms and the peripheral ring. The unique 6c-2e π-bond delocalized over the inner B_6 triangular unit also satisfy the $(4n + 2)$ rule for π-aromaticity ($n = 0$). Therefore, the B_{18}^- cluster is doubly π-aromatic, similar to the recently discovered B_{19}^- cluster.[29] Overall, the stability of isomer V (C_{3v}, $^2A_1$) of B_{18}^-, or more precisely its neutral counterpart, can be explained by its σ-aromaticity and double π-aromaticity.

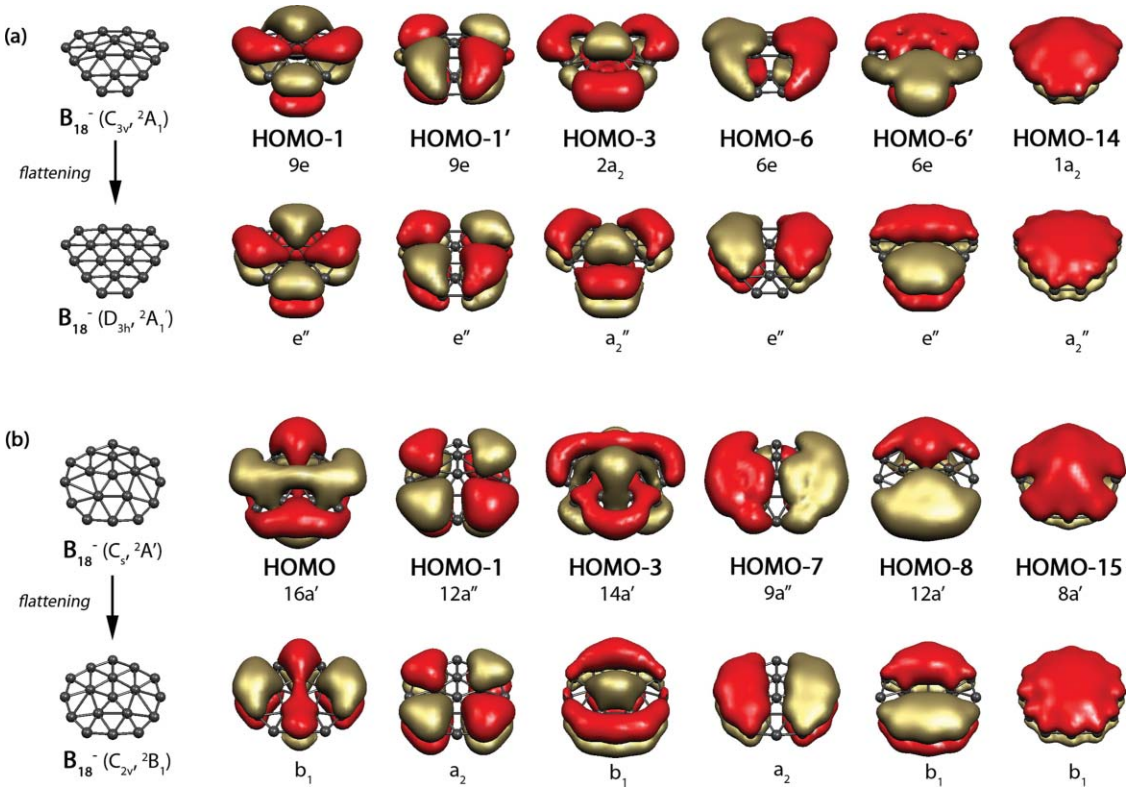

FIG. 7. (a) The π-type canonical molecular orbitals of isomer V (C_{3v}, $^2A_1$) of the B_{18}^- cluster and their representation after flattening the structure (in D_{3h} symmetry). (b) The π-type canonical molecular orbitals of isomer VI (C_s, $^2A'$) of the B_{18}^- cluster and their representation after flattening the structure (in C_{2v} symmetry).

C. Nuclear independent chemical shift analyses of isomers I, V, and VI

We performed nuclear-independent chemical shift (NICS) analyses[85] for the global minimum of B_{17}^- and the two low-lying isomers of B_{18}^-. The calculated NICSzz values of the B_{17}^- were found to be -8.2 ppm ($d = 0.2$ Å, where d represents the distance from the center of the molecule along the x axis perpendicular to the plane of the molecule), -11.9 ppm ($d = 0.4$ Å), -12.6 ppm ($d = 0.6$ Å), -10.6 ppm ($d = 0.8$ Å), and -7.6 ppm ($d = 1.0$ Å) at the optimized B3LYP/6-311+G* geometry. The negative NICSzz values are consistent with the aromatic nature of the cluster. Therefore, the NICS analysis supports our conclusion that the B_{17}^- cluster is a new member of a family of aromatic planar boron clusters. The NICSzz values of isomer V of B_{18}^- were found to be largely negative also consistent with the aromaticity of this cluster; NICSzz values range from -64.7 ppm ($d = 0$ Å) to -45.7ppm ($d = 1.0$ Å); d – distance from the center of the inner central triangle along the z axis. The above NICSzz values for B_{17}^- and $B_{18}^-$are compared to those of the prototypical organic π-aromatic molecule benzene and the recently discovered doubly π-aromatic B_{19}^- in supplementary Table S7 of the supporting information.[81]

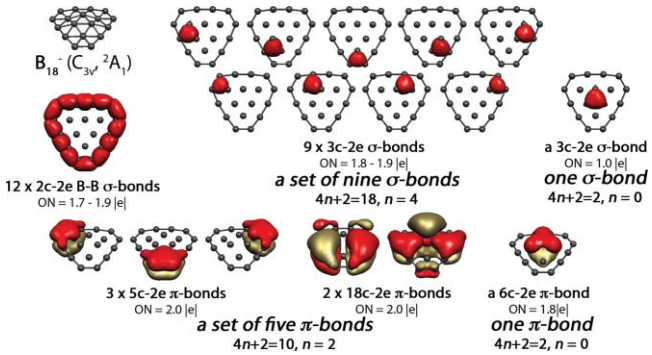

FIG. 8. Results of AdNDP analyses on the chemical bonds in the global minimum V (C_{3v}, $^2A_1$) of B_{18}^-.

VIII. CONCLUSIONS

In conclusion, we have investigated the structural and electronic properties and chemical bonding of the B_{17}^- and B_{18}^- clusters using photoelectron spectroscopy and *ab initio* calculations. Photoelectron spectral data are combined with theoretical calculations to identify the global minimum structures of the two fairly complex clusters. A perfect planar C_{2v} structure is found to be the global minimum of B_{17}^-. Chemical bonding analyses reveal that B_{17}^- possesses 10 π electrons and its five π orbitals are very similar to those of naphthalene. Thus, B_{17}^- can be viewed as an all-boron analogue of naphthalene. Two nearly degenerate quasi-planar isomers for B_{18}^- are found, which are structurally related to the two low-lying planar isomers of the B_{19}^- clusters by removing a peripheral B atom, respectively. The quasi-planarity of the two structures of the B_{18}^- cluster is found to be due to the

reduced size of the outer rings, which are too small to host the inner atoms. Chemical bonding analyses reveal that both isomers possess two sets of concentric aromatic π systems similar to that in B_{19}^- and they can be viewed as all-boron analogues of coronene. The current work has extended the concept of all-boron analogues of hydrocarbons. With these new results for B_{17}^- and B_{18}^-, we have now established systematically that anionic boron clusters from B_3^- to B_{20}^- are all planar or quasi-planar and each can be viewed as an all-boron hydrocarbon analogue.

ACKNOWLEDGMENTS

We thank Dr. W. Huang for help with the basin-hoping calculations. This work was supported by the National Science Foundation (DMR-0904034 to L.S.W. and CHE-0714851 to A.I.B.). Computer time from the Center for High Performance Computing at USU is gratefully acknowledged. The computational resource, the Uinta cluster supercomputer, was provided through the National Science Foundation under Grant No. CTS-0321170 with matching funds provided by USU.

[1] N. Vast, S. Baroni, G. Zerah, J. M. Besson, A. Polian, M. Grimsditch, and J. C. Chervin, Phys. Rev. Lett. **78**, 693 (1997).
[2] M. Fujimori, T. Nakata, T. Nakayama, E. Nishibori, K. Kimura, M. Takata, and M. Sakata, Phys. Rev. Lett. **82**, 4452 (1999).
[3] L. Hanley, J. L. Whitten, and S. L. Anderson, J. Phys. Chem. **92**, 5803 (1988).
[4] P. A. Hintz, S. A. Ruatta, and S. L. Anderson, J. Chem. Phys. **92**, 292 (1990).
[5] S. A. Ruatta, P. A. Hintz, and S. L. Anderson, J. Chem. Phys. **94**, 2833 (1991).
[6] M. B. Sowa-Resat, J. Smolanoff, A. Lapiki, and S. L. Anderson, J. Chem. Phys. **106**, 9511 (1997).
[7] V. Bonacic-Koutecky, P. Fantucci, and J. Koutecky, Chem. Rev. **91**, 1035 (1991).
[8] R. Kawai and J. H. Weare, J. Chem. Phys. **95**, 1151 (1991).
[9] R. Kawai and J. H. Weare, Chem. Phys. Lett. **191**, 311 (1992).
[10] J. M. L. Martin, J. P. François, and R. Gijbels, Chem. Phys. Lett. **189**, 529 (1992).
[11] H. Kato, K. Yamashita, and K. Morokuma, Chem. Phys. Lett. **190**, 361 (1992).
[12] I. Boustani, Int. J. Quantum Chem. **52**, 1081 (1994).
[13] I. Boustani, Chem. Phys. Lett. **233**, 273 (1995).
[14] I. Boustani, Chem. Phys. Lett. **240**, 135 (1995).
[15] A. Ricca and C. W. Bauschlicher, Jr., Chem. Phys. **208**, 233 (1996).
[16] I. Boustani, Surf. Sci. **370**, 355 (1997).
[17] I. Boustani, Phys. Rev. B **55**, 16426 (1997).
[18] J. Niu, B. K. Rao, and P. Jena, J. Chem. Phys. **107**, 132 (1997).
[19] F. L. Gu, X. Yang, A. C. Tang, H. Jiao, and P. v. R. Schleyer, J. Comput. Chem. **19**, 203 (1998).
[20] A. N. Alexandrova, A. I. Boldyrev, H. J. Zhai, and L. S. Wang, Coord. Chem. Rev. **250**, 2811 (2006).
[21] H. J. Zhai, L. S. Wang, A. N. Alexandrova, and A. I. Boldyrev, J. Chem. Phys. **117**, 7917 (2002).
[22] A. N. Alexandrova, A. I. Boldyrev, H. J. Zhai, L. S. Wang, E. Steiner, and P. W. Fowler, J. Phys. Chem. A **107**, 1359 (2003).
[23] H. J. Zhai, L. S. Wang, A. N. Alexandrova, A. I. Boldyrev, and V. G. Zakrzewski, J. Phys. Chem. A **107**, 9319 (2003).
[24] H. J. Zhai, A. N. Alexandrova, K. A. Birch, A. I. Boldyrev, and L. S. Wang, Angew. Chem. Int. Ed. **42**, 6004 (2003).
[25] H. J. Zhai, B. Kiran, J. Li, and L. S. Wang, Nature Mater. **2**, 827 (2003).
[26] A. N. Alexandrova, A. I. Boldyrev, H. J. Zhai, and L. S. Wang, J. Phys. Chem. A **108**, 3509 (2004).
[27] A. P. Sergeeva, D. Yu. Zubarev, H. J. Zhai, A. I. Boldyrev, and L. S. Wang, J. Am. Chem. Soc. **130**, 7244 (2008).
[28] B. Kiran, S. Bulusu, H. J. Zhai, S. Yoo, X. C. Zeng, and L. S. Wang, Proc. Natl. Acad. Sci. U.S.A. **102**, 961 (2005).
[29] W. Huang, A. P. Sergeeva, H. J. Zhai, B. B. Averkiev, L. S. Wang, and A. I. Boldyrev, Nat. Chem. **2**, 202 (2010).
[30] A. N. Alexandrova, H. J. Zhai, L. S. Wang, and A. I. Boldyrev, Inorg. Chem. **43**, 3552 (2004).
[31] A. N. Alexandrova, A. I. Boldyrev, H. J. Zhai, and L. S. Wang, J. Chem. Phys. **122**, 054313 (2005).
[32] H. J. Zhai, L. S. Wang, D. Yu. Zubarev, and A. I. Boldyrev, J. Phys. Chem. A **110**, 1689 (2006).
[33] L. M. Wang, W. Huang, B. B. Averkiev, A. I. Boldyrev, and L. S. Wang, Angew. Chem. Int. Ed. **46**, 4550 (2007)
[34] B. B. Averkiev, D. Yu. Zubarev, L. M. Wang, W. Huang, L. S. Wang, and A. I. Boldyrev, J. Am. Chem. Soc. **130**, 9248 (2008).
[35] B. B. Averkiev, L. M. Wang, W. Huang, L. S. Wang, and A. I. Boldyrev, Phys. Chem. Chem. Phys. **11**, 9840 (2009).
[36] H. J. Zhai, S. D. Li, and L. S. Wang, J. Am. Chem. Soc. **129**, 9254 (2007).
[37] S. D. Li, H. J. Zhai, and L. S. Wang, J. Am. Chem. Soc. **130**, 2573 (2008).
[38] H. J. Zhai, C. Q. Miao, S. D. Li, and L. S. Wang, J. Phys. Chem. A **114**, 12155 (2010).
[39] E. Oger, N. R. M. Crawford, R. Kelting, P. Weis, M. M. Kappes, and R. Ahlrichs, Angew. Chem. Int. Ed. **46**, 8503 (2007).
[40] W. An, S. Bulusu, Y. Gao, and X. C. Zeng, J. Chem. Phys. **124**, 154310 (2006).
[41] L. L. Pan, J. Li, and L. S. Wang, J. Chem. Phys. **129**, 024302 (2008).
[42] J. E. Fowler and J. M. Ugalde, J. Phys. Chem. A **104**, 397 (2000).
[43] J.-i. Aihara, J. Phys. Chem. A **105**, 5486 (2001).
[44] J.-i. Aihara, H. Kanno, and T. Ishida, J. Am. Chem. Soc. **127**, 13324 (2005).
[45] P. W. Fowler and B. R. Gray, Inorg. Chem. **46**, 2892 (2007).
[46] D. Yu. Zubarev and A. I. Boldyrev, J. Comput. Chem. **28**, 251 (2007).
[47] D. Yu. Zubarev, A. P. Sergeeva, and A. I. Boldyrev, in *Chemical Reactivity Theory. A Density Functional View*, edited by P. K. Chattaraj (CRC Press, New York, 2009), pp. 439–452.
[48] L. S. Wang, H. S. Cheng, and J. Fan, J. Chem. Phys. **102**, 9480 (1995).
[49] B. B. Averkiev, "Geometry and electronic structure of doped clusters via the Coalescence Kick method," Ph.D. dissertation (Utah State University, Logan, Utah, 2009).
[50] M. Saunders, J. Comput. Chem. **25**, 621 (2004).
[51] P. P. Bera, K. W. Sattelmeyer, M. Saunders, H. F. Schaefer, and P. v. R. Schleyer, J. Phys. Chem. A **110**, 4287 (2006).
[52] D. J. Wales and J. P. K. Doye, J. Phys. Chem. A **101**, 5111 (1997).
[53] D. J. Wales and H. A. Scheraga, Science **285**, 1368 (1999).
[54] S. Yoo and X. C. Zeng, J. Chem. Phys. **119**, 1442 (2003).
[55] S. Yoo and X. C. Zeng, Angew. Chem. Int. Ed. **44**, 1491 (2005).
[56] A. D. Becke, J. Chem. Phys. **98**, 5648 (1993).
[57] S. H. Vosko, L. Wilk, and M. Nusair, Can. J. Phys. **58**, 1200 (1980).
[58] C. Lee, W. Yang, and R. G. Parr, Phys. Rev. B **37**, 785 (1988).
[59] J. S. Binkley, J. A. Pople, and W. J. Hehre, J. Am. Chem. Soc. **102**, 939 (1980).
[60] X. B. Wang, J. B. Nicholas, and L. S. Wang, J. Chem. Phys. **113**, 10837 (2000).
[61] X. B. Wang, A. P. Sergeeva, J. Yang, X. P. Xing, A. I. Boldyrev, and L. S. Wang, J. Phys. Chem. A **113**, 5567 (2009).
[62] M. S. Gordon, J. S. Binkley, J. A. Pople, W. J. Pietro, and W. J. Hehre, J. Am. Chem. Soc. **104**, 2797 (1982).
[63] W. J. Pietro, M. M. Francl, W. J. Hehre, D. J. Defrees, J. A. Pople, and J. S. Binkley, J. Am. Chem. Soc. **104**, 5039 (1982).
[64] T. Clark, J. Chandrasekhar, G. W. Spitznagel, and P. v. R. Schleyer, J. Comput. Chem. **4**, 294 (1983).
[65] J. Cizek, Adv. Chem. Phys. **14**, 35 (1969).
[66] G. D. Purvis and R. J. Bartlett, J. Chem. Phys. **76**, 1910 (1982).
[67] K. Raghavachari, G. W. Trucks, J. A. Pople, and M. Head-Gordon, Chem. Phys. Lett. **157**, 479 (1989).
[68] L. S. Cederbaum, J. Phys. B **8**, 290 (1975).
[69] J. V. Ortiz, Int. J. Quantum Chem., Quantum Chem. Symp. **36**(S23), 321 (1989).
[70] J. S. Lin and J. V. Ortiz, Chem. Phys. Lett. **171**, 197 (1990).
[71] V. G. Zakrzewski, J. V. Ortiz, J. A. Nichols, D. Heryadi, D. L. Yeager, and J. T. Golab, Int. J. Quantum Chem. **60**, 29 (1996).
[72] R. Bauernschmitt and R. Ahlrichs, Chem. Phys. Lett. **256**, 454 (1996).
[73] M. E. Casida, C. Jamorski, K. C. Casida, and D. R. Salahub, J. Chem. Phys. **108**, 4439 (1998).

[74]M. J. Frisch, G. W. Trucks, H. B. Schlegel *et al.*, GAUSSIAN 03, Revision D.01, Gaussian, Inc., Wallingford, CT, 2004.
[75]G. Schaftenaar, MOLDEN 3.4, CAOS/CAMM Center, The Netherlands, 1998.
[76]D. Yu. Zubarev and A. I. Boldyrev, Phys. Chem. Chem. Phys. **10**, 5207 (2008).
[77]D. Yu. Zubarev and A. I. Boldyrev, J. Org. Chem. **73**, 9251 (2008).
[78]D. Yu. Zubarev and A. I. Boldyrev, J. Phys. Chem. A **113**, 866 (2009).
[79]A. P. Sergeeva and A. I. Boldyrev, Comm. Inorg. Chem. **31**, 2 (2010).
[80]S. Portmann, MOLEKEL, Version 4.3, Swiss National Supercomputing Centre/Swiss Federal Institute of Technology, Zurich, 2002.
[81]See supplementary material at http://dx.doi.org/10.1063/1.3599452 for calculated molecular properties of clusters.
[82]We optimized the geometry and performed frequency calculations for the B_2H_4 (D_{2d}, $^1A_1$) molecule. The optimized B-B distance in this molecule was 1.629 Å.
[83]J. O. C. Jimenez-Halla, R. Islas, T. Heine, and G. Merino, Angew. Chem. Int. Ed. **49**, 5668 (2010).
[84]C. Romanescu, A. P. Sergeeva, W. L. Li, A. I. Boldyrev, and L. S. Wang, J. Am. Chem. Soc., **133**, 8646 (2011).
[85]P. v. R. Schleyer, C. Maerker, A. Dransfeld, H. Jiao, and N. J. R. v. E. Hommes, J. Am. Chem. Soc. **118**, 6317 (1996).